



HAL
open science

Atomic Structure and Dynamics of Unusual and Wide-Gap Phase-Change Chalcogenides: A GeTe₂ Case

Takeshi Usuki, Chris Benmore, Andrey Tverjanovich, Sergei Bereznev, Maxim Khomenko, Anton Sokolov, Daniele Fontanari, Koji Ohara, Maria Bokova, Mohammad Kassem, et al.

► To cite this version:

Takeshi Usuki, Chris Benmore, Andrey Tverjanovich, Sergei Bereznev, Maxim Khomenko, et al.. Atomic Structure and Dynamics of Unusual and Wide-Gap Phase-Change Chalcogenides: A GeTe₂ Case. *physica status solidi (RRL) - Rapid Research Letters*, 2024, pp.2300482. 10.1002/pssr.202300482. hal-04443961

HAL Id: hal-04443961

<https://ulco.hal.science/hal-04443961>

Submitted on 7 Feb 2024

HAL is a multi-disciplinary open access archive for the deposit and dissemination of scientific research documents, whether they are published or not. The documents may come from teaching and research institutions in France or abroad, or from public or private research centers.

L'archive ouverte pluridisciplinaire **HAL**, est destinée au dépôt et à la diffusion de documents scientifiques de niveau recherche, publiés ou non, émanant des établissements d'enseignement et de recherche français ou étrangers, des laboratoires publics ou privés.

Atomic Structure and Dynamics of Unusual and Wide-Gap Phase-Change Chalcogenides: A GeTe₂ Case

Takeshi Usuki, Chris J. Benmore, Andrey Tverjanovich, Sergei Bereznev, Maxim Khomenko, Anton Sokolov, Daniele Fontanari, Koji Ohara, Maria Bokova, Mohammad Kassem, and Eugene Bychkov*

Brain-inspired computing, reconfigurable optical metamaterials, photonic tensor cores, and many other advanced applications require next-generation phase-change materials (PCMs) with better energy efficiency and a wider thermal and spectral range for reliable operations. Germanium ditelluride (GeTe₂), with higher thermal stability and a larger bandgap compared to current benchmark PCMs, appears promising for THz metasurfaces and the controlled crystallization of atomically thin 2D materials. Using high-energy X-Ray diffraction supported by first-principles simulation, the atomic structure in semiconducting pulsed laser deposition films and metallic high-temperature liquids is investigated. The results suggest that the structural and chemical metastability of GeTe₂, leading to disproportionation into GeTe and Te, is related to high internal pressure during a semiconductor–metal transition, presumably occurring in the supercooled melt. Similar phenomena are expected for canonical GeS₂ and GeSe₂ under high temperatures and pressures.

circuits, and many other advanced applications.^[1–6] Further progress requires next-generation PCMs with improved energy efficiency and a wider temperature and spectral range compared to classical benchmark systems such as GeTe–Sb₂Te₂ and doped Sb₂Te. Germanium monotelluride GeTe has been extensively studied for PCM applications; however, its ditelluride counterpart GeTe₂ is relatively unknown. Recently, we succeeded in obtaining bulk glassy GeTe₂ and investigated its thermal, electrical, and structural properties using diffraction techniques and first-principles simulations.^[7] Additionally, pulsed laser deposition (PLD) films were prepared and appear to be promising candidates for reconfigurable THz metasurfaces.^[8] The SET and RESET logic states of GeTe₂ PLD films demonstrated high electrical and optical contrast, a wider optical bandgap, and thermal stability compared to GeTe. Simultaneously, sputter-deposited amorphous GeTe₂ thin films were found to be effective precursors of metastable van der Waals 2D compounds with great potential for future electronics.^[9] Nevertheless, the structural features of glassy or amorphous thin films have not been studied, and neither

1. Introduction

Phase-change materials (PCMs) based on tellurides are well-established functional systems for optical nonvolatile memories, neuromorphic computing, light or electrically controlled reconfigurable optical metamaterials, integrated photonic


trical and optical contrast, a wider optical bandgap, and thermal stability compared to GeTe. Simultaneously, sputter-deposited amorphous GeTe₂ thin films were found to be effective precursors of metastable van der Waals 2D compounds with great potential for future electronics.^[9] Nevertheless, the structural features of glassy or amorphous thin films have not been studied, and neither

T. Usuki
Faculty of Science
Yamagata University
Yamagata 990-8560, Japan

C. J. Benmore
X-ray Science Division
Advanced Photon Source
Argonne National Laboratory
Argonne, IL 60439, USA

A. Tverjanovich
Institute of Chemistry
St. Petersburg State University
198504 St. Petersburg, Russia

S. Bereznev
Department of Materials and Environmental Technology
Tallinn University of Technology
19086 Tallinn, Estonia

 The ORCID identification number(s) for the author(s) of this article can be found under <https://doi.org/10.1002/pssr.202300482>.

DOI: 10.1002/pssr.202300482

S. Bereznev
Virumaa College
Tallinn University of Technology
30322 Kohtla-Järve, Estonia

M. Khomenko
NRC “Kurchatov Institute”
140700 Shatura, Moscow Region, Russia

M. Khomenko
Laboratory of Biophotonics
Tomsk State University
634050 Tomsk, Russia

A. Sokolov, D. Fontanari, M. Bokova, M. Kassem, E. Bychkov
Laboratoire de Physico-Chimie de l'Atmosphère
Université du Littoral Côte d'Opale
59140 Dunkerque, France
E-mail: bychkov@univ-littoral.fr

K. Ohara
Faculty of Materials for Energy
Shimane University
1060, Nishi-Kawatsu-Cho, Matsue, Shimane 690-8504, Japan

has the structural evolution of molten GeTe_2 , presumably exhibiting a semiconductor–metal transition above the melting point.

The primary objective of the present report consists of high-energy X-ray diffraction (HE-XRD) studies of glassy GeTe_2 PLD thin films and bulk high-temperature liquids over a wide temperature range to elucidate the atomic structure of both semiconducting and metallic germanium ditelluride. The diffraction studies will be completed by first-principles molecular dynamics (FPMD) to gain a deep insight into the nature of the semiconductor–metal transition and the underlying structural evolution. The results will be compared with reported atomic structures and dynamics in widely studied canonical GeS_2 and GeSe_2 glasses and liquids, thereby unraveling the role of tellurium in germanium dichalcogenides. This comparison enables us to follow the changes in both macroscopic properties and microscopic structure, going from the purely semiconducting GeS_2 to the metallic GeTe_2 liquid, passing through the stages of semiconducting and then metallic GeSe_2 . Special attention will be given to the high internal pressure in dense metallic GeTe_2 , providing an explanation for the structural and chemical metastability of this compound in both glassy and liquid forms.

2. Results and Discussions

2.1. Semiconductor–Metal Transition and High Internal Pressure in Molten GeTe_2

The glassy PLD film of GeTe_2 has the maximum glass transition temperature, $T_g = 478$ K, in the system $\text{Ge}_x\text{Te}_{1-x}$ (Figure 1a,b),

followed by intense exothermic crystallization. In contrast to the vast majority of typical PCM, the glass transition is clearly visible (inset in Figure 1a) and appears to be slightly higher than that for bulk glassy GeTe_2 , possibly due to a higher quenching rate in the PLD film. The overall shape of $T_g(x)$ in the Ge–Te binaries resembles that in their sulfide^[10] and selenide counterparts (Figure 1c,d). However, it should be noted that a wide range of T_g values for amorphous GeTe exists, depending on the differential scanning calorimetry (DSC) rate and preliminary annealing procedures.^[11,12]

The density of glassy GeTe_2 (5.33 g cm^{-3}) appears to be markedly lower than the liquid density ($\approx 5.6 \text{ g cm}^{-3}$ at 850 K),^[13] suggesting that a semiconductor–metal transition occurs in the supercooled state (the hypothetical dashed line in Figure 2a, consistent with the observed trends in Ge–Te liquids^[13]). The metallic conductivity of molten GeTe_2 ($\approx 3000 \text{ S cm}^{-1}$)^[14] confirms this conclusion, as shown in Figure 2b.

In contrast, germanium disulfide remains semiconducting up to the highest accessible temperature, while germanium diselenide starts to exhibit the beginning of a semiconductor–metal transition above 1100 K. The density of molten GeSe_2 decreases above T_g , reveals a minimum at ≈ 1050 K, and finally increases at higher temperatures (Figure 2a). Simultaneously, a semiconducting liquid GeSe_2 reveals a rapid transient conductivity increase, reaching 200 S cm^{-1} above 1100 K (Figure 2b).^[15,16]

The reported neutron diffraction measurements of molten GeTe_2 ,^[17–19] previous studies of bulk glassy germanium

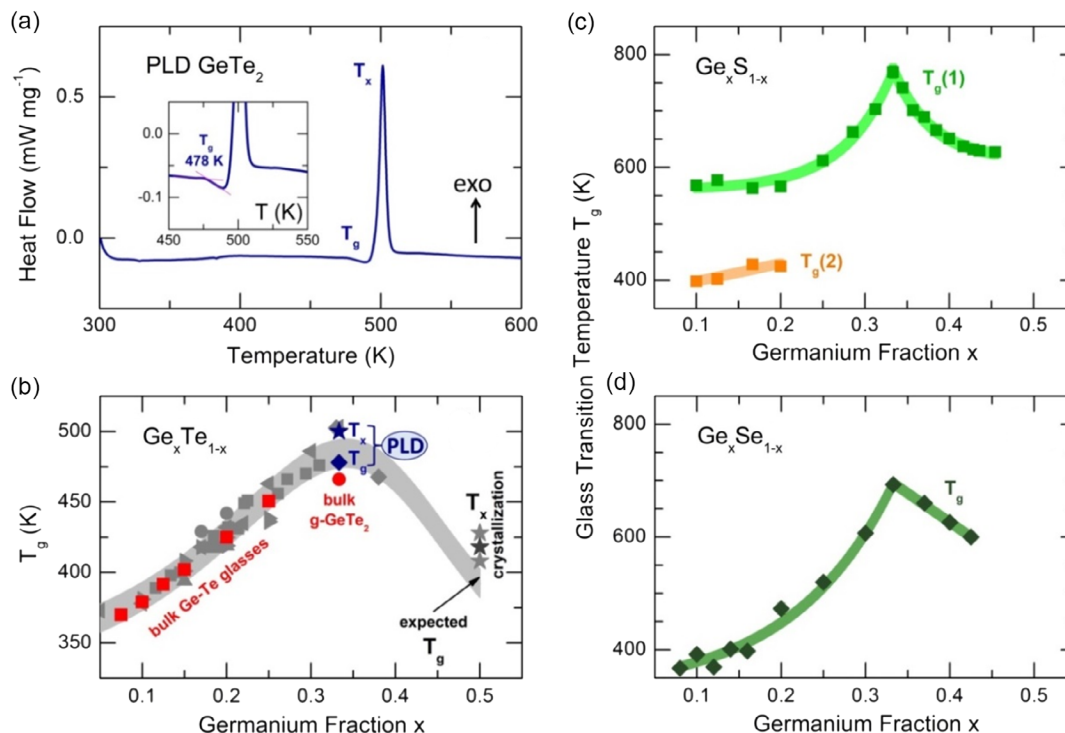


Figure 1. Thermal properties of glassy germanium chalcogenides: a) a DSC trace of a GeTe_2 PLD film, the inset shows the enlarged glass transition part; b) glass transition temperatures for glassy $\text{Ge}_x\text{Te}_{1-x}$ alloys (Ref. [7] and studies therein, our data are highlighted in red (bulk glasses) and blue (GeTe_2 PLD)); c) glass transition temperatures in the $\text{Ge}_x\text{S}_{1-x}$ system,^[10] the second glass transition $T_g(2)$ in phase-separated glasses at $x \leq 0.2$ corresponds to a sulfur-rich phase; and d) glass transition temperatures in the $\text{Ge}_x\text{Se}_{1-x}$ system (this work). See the text for further details.

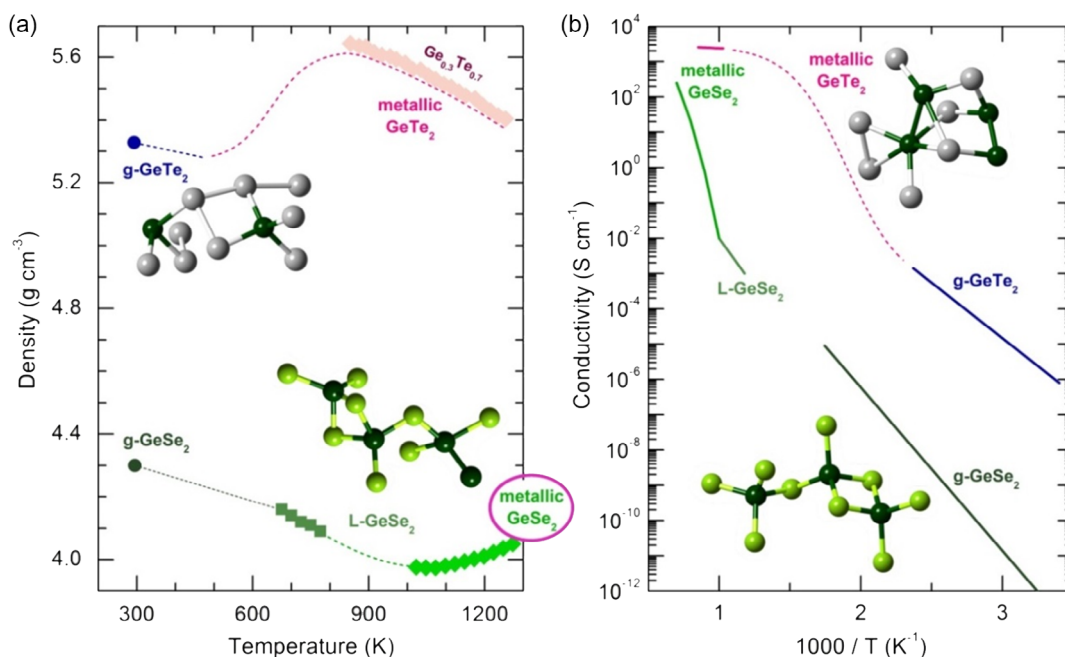


Figure 2. a) Density and b) conductivity of GeTe₂ and GeSe₂ over a wide temperature range. The insets represent structural motifs of glassy and metallic GeTe₂ (ref. [7] and this work) and glassy/liquid GeSe₂.^[32,38–40] The density of liquid Ge_{0.3}Te_{0.7} is taken from ref. [13]. Densities of semiconducting and metallic liquids GeSe₂ were reported in Refs. [15,52]. The conductivities of liquid GeTe₂ and GeSe₂ were taken from refs. [14–16]. The dashed lines represent the expected behavior.

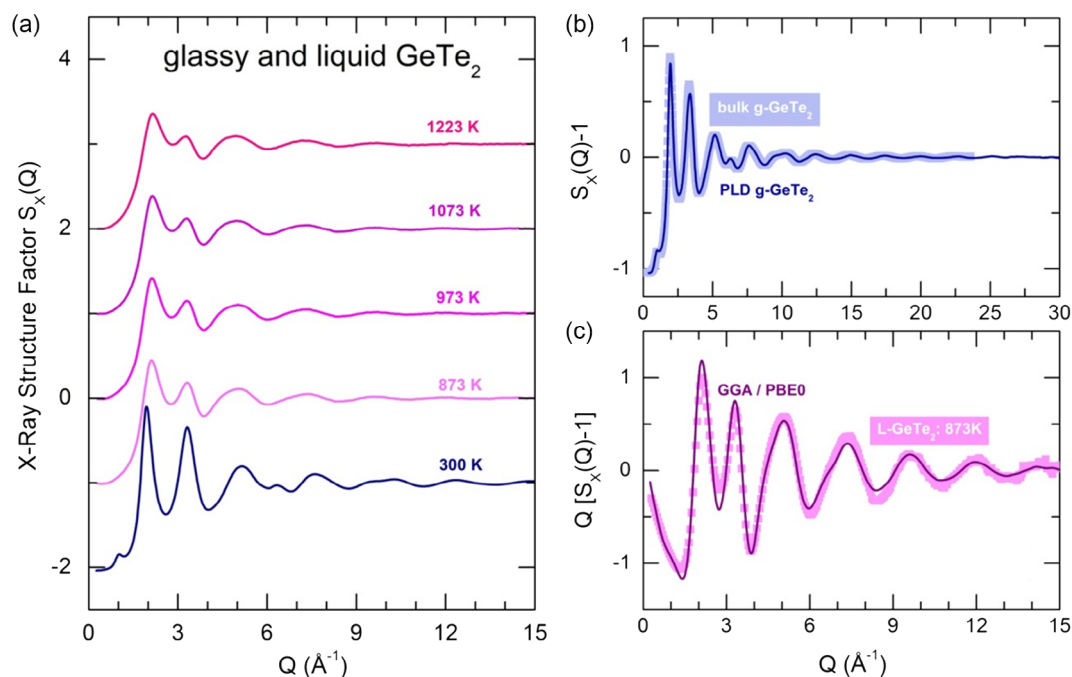


Figure 3. High-energy X-Ray diffraction data of glassy and liquid GeTe₂ in *Q*-space: a) structure factors $S_x(Q)$ over a wide *T* range from room temperature to 1223 K; b) $S_x(Q)$ for bulk glassy GeTe₂^[7] and PLD vitreous thin film (this work); c) interference function $Q[S_x(Q) - 1]$ for L-GeTe₂ at 873 K and its FPMD replica simulated using a GGA/PBE0 hybrid functional.

ditelluride,^[7] and the present HE-XRD results of PLD g-GeTe₂ and liquid L-GeTe₂ jointly illustrate a drastic structural evolution from semiconducting-to-metallic forms. The X-Ray structure

factors $S_x(Q)$ over a wide temperature range are shown in **Figure 3a**. The PLD sample reveals a nearly identical $S_x(Q)$ compared to bulk glassy GeTe₂ (Figure 3b), which exhibits a small

first sharp diffraction peak (FSDP) at $Q_0 \approx 1.0 \text{ \AA}^{-1}$ and distinct high- Q oscillations up to 30 \AA^{-1} . Above melting, the FSDP nearly disappears, while the intense first- and second-principal peaks (PP1 and PP2) at $Q_1 = 1.95 \text{ \AA}^{-1}$ and $Q_2 = 3.31 \text{ \AA}^{-1}$ broaden and decrease in amplitude. The high- Q oscillations also exhibit damping and a shift to lower scattering vectors, indicating an increase in interatomic distances. In addition, the relative amplitude of PP1 becomes more intense compared to PP2, a characteristic feature typical of metallic alloys.^[20–22] As expected, FPMD in the general gradient approximation (GGA) with hybrid functional PBE0^[23,24] well reproduces both room-temperature and high-temperature diffraction results, as shown in Figure 3c for the metallic liquid.

The FSDP evolution with increasing temperature is coherent with the semiconductor–metal transition and the transition to a more dense metallic liquid above melting. Similar to diffraction patterns observed in glasses and liquids under high pressure,^[25–27] the FSDP shifts to higher Q with a simultaneous decrease in amplitude A_0 (Figure 4). These changes are hardly visible in the X-Ray data, as the dominant Te–Te contribution to $S_X(Q)$ with a large Q -dependent weighing factor, $w_{\text{Te–Te}}^X(Q) = 0.6209$, does not exhibit any contribution to the FSDP (see Figure S1, Supporting Information). In contrast, the reported neutron data^[17–19] are more sensitive to FSDP changes, with $w_{\text{Te–Te}}^N/w_{\text{Ge–Ge}}^X(Q) = 0.55$, resulting in a pronounced FSDP (Figure 4). Some differences in the FSDP parameters between neutron and X-Ray results are attributed to the Ge–Ge and Ge–Te weightings ($w_{\text{Ge–Ge}}^N/w_{\text{Ge–Ge}}^X(Q) = 3.78$ and $w_{\text{Ge–Te}}^N/w_{\text{Ge–Te}}^X(Q) = 1.45$), as these two correlations contribute to the FSDP (Figure S1, Supporting Information).

Summarizing, the FSDP evolution indicates the existence of high internal pressure in metallic GeTe₂ melts. Similar behavior was observed in other PCM materials,^[28–30] suggesting that this phenomenon may be typical for semiconductor–metal transitions and phase-change switching. In particular, it seems to be related to a very unusual observation of nanotectonic compression, that is, a simultaneous cocrystallization of ambient and high-pressure polymorphs on heating of glassy GaTe₃.^[31] We should also note a shift of the FSDP position to a higher Q for liquid GeSe₂ above 1000 K^[32] occurring simultaneously with a density increase and the onset of metallization (Figure 2).

2.2. Local Structure in Semiconducting and Metallic GeTe₂

The disappearance of intermediate-range order, characteristic of semiconducting g-GeTe₂ and reflected by the FSDP upon heating above melting, is accompanied by dramatic changes in the local Ge and Te environment, as deduced using correlation functions in r -space. Figure 5 represents the total correlation functions $T_X(r)$ over a wide range from room temperature to 1223 K, obtained by the usual Fourier transform of $S_X(Q)$. The PLD film shows nearly identical $T_X(r)$ to bulk glassy GeTe₂, and these are well reproduced by FPMD simulations with the GGA/PBE0 hybrid functional (Figure 5c). The asymmetric nearest-neighbor (NN) peak at 2.64 Å comprises three contributions: dominant Ge–Te correlations with a partial coordination number $N_{\text{Ge–Te}} = 3.40 \pm 0.10$, significant Te–Te homopolar atomic pairs ($N_{\text{Te–Te}} = 0.61 \pm 0.03$), and weak Ge–Ge contacts ($N_{\text{Ge–Ge}} = 0.13 \pm 0.03$), which are hardly visible in Figure 5b. A broad asymmetric second-neighbor peak at 4.22 Å is composed

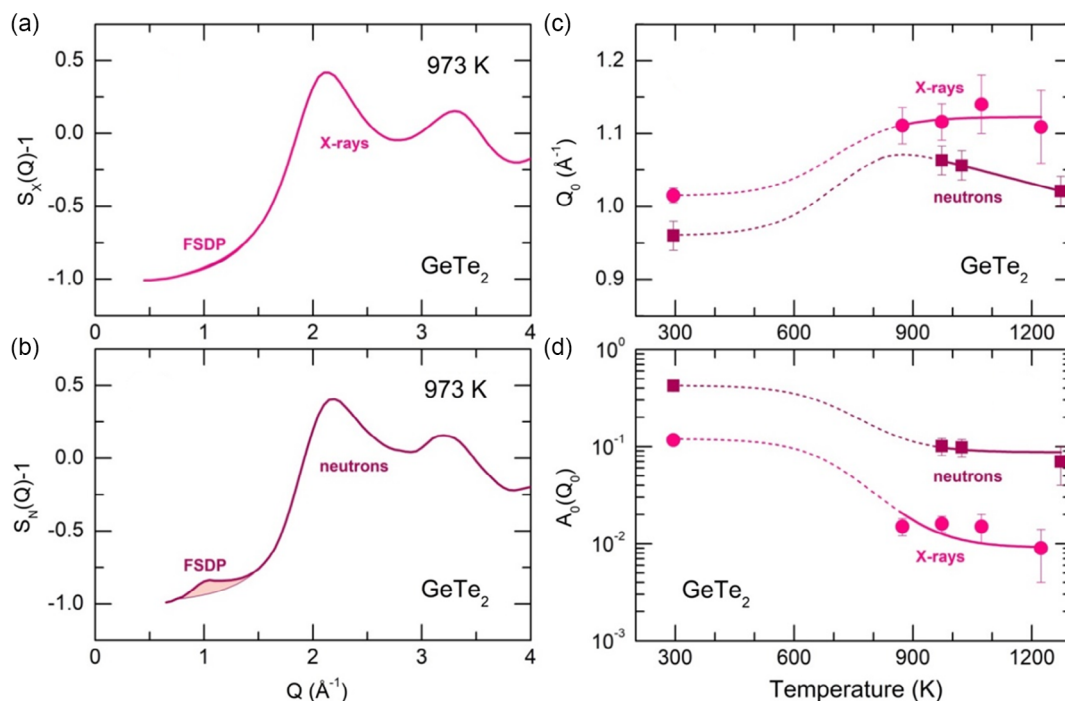


Figure 4. FSDP parameters in glassy and liquid GeTe₂: a) X-Ray (this work) and b) neutron^[17] structure factors at 973 K and low $Q \leq 4 \text{ \AA}^{-1}$; the isolation of the FSDP at $Q_0 \approx 1 \text{ \AA}^{-1}$ is shown applying the Voigt function as the background beneath the FSDP; c) peak positions $Q_0(T)$ and d) FSDP amplitudes $A_0(T)$ as a function of temperature for X-Ray (this work) and neutron^[17–19] data.

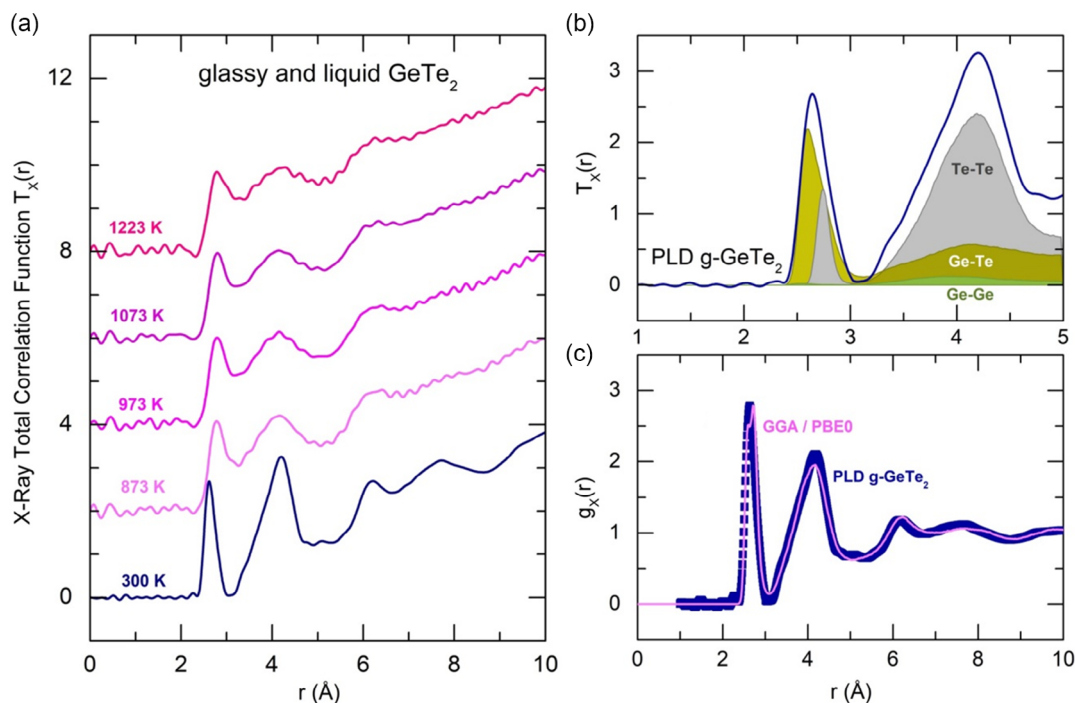


Figure 5. X-Ray diffraction data of glassy and liquid GeTe_2 in r -space: a) total correlation functions $T_X(r)$ over a wide T -range; b) experimental $T_X(r)$ for a glassy PLD film GeTe_2 and X-Ray weighted FPMD partials (Ge–Ge, Ge–Te, and Te–Te highlighted in green, mustard and gray, respectively); c) experimental and FPMD-derived pair-distribution functions $g_X(r)$ for a $g\text{-GeTe}_2$ PLD film.

of the same correlations but the Te–Te second neighbors become the most intense. The NN and second-neighbor correlations are well separated, revealing a deep minimum at $\approx 3.1 \text{ \AA}$.

The metallic liquids display broad and increasingly overlapping peaks between 2 and 5 \AA . The distant correlations at 6.2 and 7.7 \AA , observed in $g\text{-GeTe}_2$, have almost vanished, giving way to a nearly flat and featureless background. The last finding is consistent with the disappearance of intermediate-range order, as reflected by the FSDP. In addition to these qualitative observations, we note remarkable quantitative differences. First, the maximum of the NN peak shifts from 2.64 to 2.78 \AA , indicating significant variations in the local structure (see **Figure 6**). Glassy GeTe_2 exhibits a strongly asymmetric Ge–Te NN peak, attributed to the shorter tetrahedral $\text{Ge}_{4F}\text{-Te}$ bond (2.60 \AA) and longer trigonal $\text{Ge}_{3F}\text{-Te}$ bond (2.77 \AA) lengths (Figure 6a). The derived difference, $\Delta r_{3F-4F} = 0.17 \text{ \AA}$, is typical for tetrahedral and trigonal interatomic distances in GeS_2/GeS ($\Delta r = 0.22 \text{ \AA}$) and $\text{GeSe}_2/\text{GeSe}$ ($\Delta r = 0.20 \text{ \AA}$) crystalline compounds.^[33–35] We note that orthorhombic GeS and GeSe, as well as rhombohedral GeTe, are characterized by a significant Peierls distortion. The trigonal Ge coordination is associated with short $\text{Ge}_{3F}\text{-X}$ separations. However, the derived $\text{Ge}_{3F}\text{-Te}$ distance is slightly smaller than the short Ge–Te(S) bond length in rhombohedral GeTe (2.827 \AA).^[36] Additional discussions on the local germanium and tellurium environment can be found in the Supporting Information, including Figure S2, Supporting Information.

The NN feature of the Ge–Te partial function $T_{\text{Ge-Te}}(r)$ in metallic liquid GeTe_2 follows the entire NN peak, becoming broad, shifting to higher r , and overlapping with the second neighbors (Figure 6b). The asymmetric NN feature also

comprises two equally populated contributions: shorter Ge–Te(S) at 2.78 \AA and longer Ge–Te(L) at 3.12 \AA . These two Ge–Te correlations are also slightly smaller (by $\approx 0.05 \text{ \AA}$) than the short/long Peierls pair in rhombohedral GeTe. The shift to higher distances compared to glassy GeTe_2 is typically associated with an increasing coordination number in metallic liquid. Gaussian fitting of $T_{\text{Ge-Te}}(r)$ or simple integration is consistent with this assumption: $N_{\text{Ge-Te(S)}} \approx N_{\text{Ge-Te(L)}}$, and $4.2(2) \leq N_{\text{Ge-Te(S)}} + N_{\text{Ge-Te(L)}} \leq 4.5(2)$ versus $N_{\text{Ge}_{4F}\text{-Te}} \approx N_{\text{Ge}_{3F}\text{-Te}}$, and $3.4(1) \leq N_{\text{Ge}_{4F}\text{-Te}} + N_{\text{Ge}_{3F}\text{-Te}} \leq 3.5(1)$. In addition, a remarkable increase in homopolar bonds is observed above melting: $N_{\text{Ge-Ge}} = 0.80 \pm 0.05$ and $N_{\text{Te-Te}} = 1.14 \pm 0.10$, resulting in enhanced Ge and Te local coordination (see Figure 6d).

The experimental diffraction results and FPMD simulations indicate partial disproportionation in germanium ditelluride, $\text{GeTe}_2 \rightleftharpoons \text{GeTe} + \text{Te}$, in the glassy/amorphous state. This reaction is complete above melting, consistent with the phase diagram.^[37] The metallic liquid appears to be denser than rhombohedral GeTe, as evidenced by slightly smaller Ge–Te NN correlations and remarkably shorter Ge–Te second neighbors ($\approx 4.08 \text{ \AA}$ in the liquid, Figure 6b, compared to 5.07 \AA in the crystal^[36]). However, the overall germanium coordination is reduced in metallic GeTe_2 in comparison with the distorted octahedral germanium environment in crystalline GeTe. The typical structural motifs of semiconducting and metallic GeTe_2 are illustrated in the insets of Figure 2.

It is worth mentioning that tetrahedral germanium coordination remains intact in molten GeS_2 and GeSe_2 .^[18,32,38–40] While there is no surprise for semiconducting germanium disulfide, the onset of metallization above 1100 K in liquid GeSe_2 allows

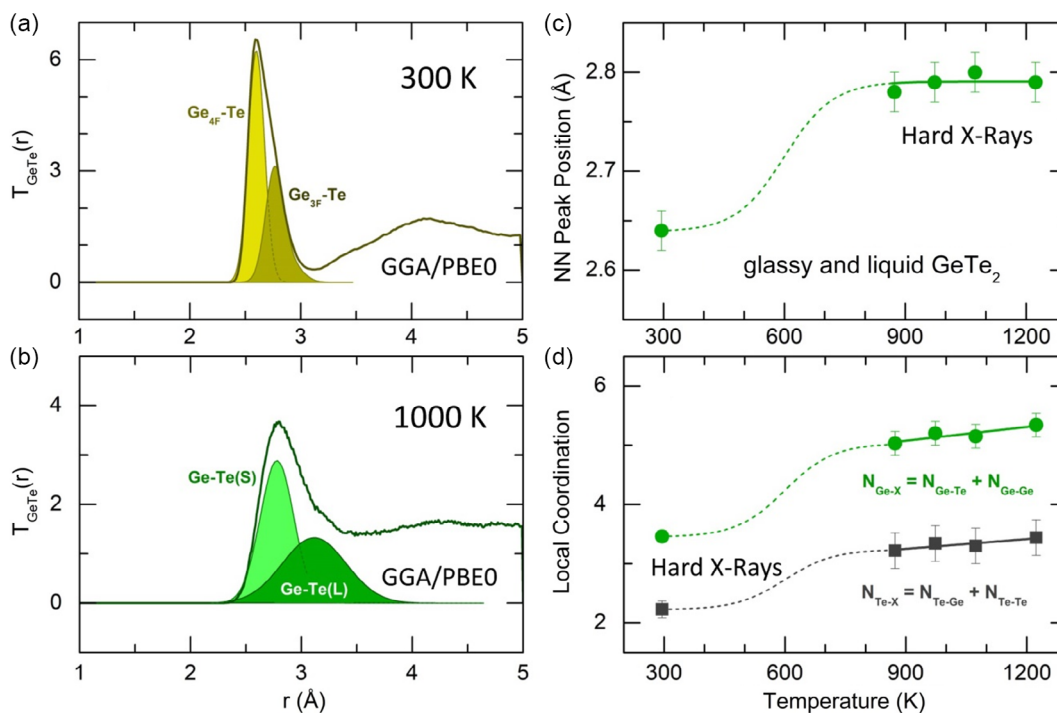


Figure 6. Structural evolution of semiconducting g-GeTe₂ and its metallic liquid above melting: fitting of FPMD-derived $T_{\text{Ge-Te}}(r)$ partials at a) 300 K and b) 1000 K; c) experimental NN peak position, and d) local Ge and Te coordination as a function of temperature.

for a possible structural transformation. However, it appears that this structural change may occur at a higher temperature, coinciding with the upcoming density maximum. At lower temperatures, both experimental and FPMD results reveal only the presence of enhanced chemical disorder, characterized by an increase in Ge–Ge and Se–Se homopolar bonds, as partly shown in the inset in Figure 2.

The presence of high internal pressure in metallic liquid GeTe₂ may be the cause of the structural and chemical metastability of germanium ditelluride. If this assumption holds true, one would expect a disproportionation reaction under high temperature and pressure for both GeSe₂ and GeS₂. Further experiments and/or FPMD simulations could be useful to either confirm or disapprove this hypothesis.

2.3. Viscosity of Germanium Dichalcogenides

The viscosity $\eta(T)$ of the vast majority of molten chalcogenides can be approximated by a few well-known models as the Vogel–Tammann–Fulcher approximation^[41] or the Mauro–Yue–Ellison–Gupta–Allan (MYEGA) relationship.^[42]

$$\log \eta(T) = \log \eta_0 + \left[\log \eta(T_g) - \log \eta_0 \right] \frac{T_g}{T} \exp \left[\left(\frac{m}{\log \eta(T_g) - \log \eta_0} \right) \left(\frac{T_g}{T} - 1 \right) \right] \quad (1)$$

where m is the fragility index, $m = [\partial \log \eta / \partial (T_g/T)]_{T=T_g}$, η_0 and $\eta(T_g) = 10^{12}$ Pa·s are the viscosity values at $T = \infty$ and

the glass transition temperature T_g , respectively. The fragility index m varies from $m = 16$ –17 for strong liquids as SiO₂ or GeO₂, revealing a nearly Arrhenius behavior, to $m > 100$ for strongly fragile fluids as organic solvents.^[43,44] Phase-change tellurides are typically fragile liquids with $m > 50$.^[45–47] Additionally, for some PCMs such as Ge₃Sb₆Te₅, a well-documented fragile-to-strong transition has been observed, spanning over 16 orders of magnitude in viscosity.^[48]

Molten germanium dichalcogenides (GeS₂, GeSe₂, and GeTe₂) exhibit a very systematic viscosity trend, wherein viscosity $\eta(T)$ decreases, and the fragility index m increases with the chalcogen atomic number (Figure 7). The viscosity of GeSe₂^[49–51] does not follow a single MYEGA equation. Instead, it can be described as exhibiting both high-temperature “metallic” viscosity with enhanced fragility ($m = 90$) and a semiconducting viscosity with lower $m = 69$. The nonmonotonic transition between these two states corresponds to a semiconductor–metal transition, evidenced by a density increase^[15,52] and high conductivity ($\sigma > 100$ S cm^{−1}) observed above 1100 K.^[15,16] Similar behavior might be detected for the supercooled hypothetical semiconducting GeTe₂, but this viscosity range is inaccessible both experimentally and using FPMD simulations. We also cannot exclude the possibility of a fragile-to-strong transition.

3. Conclusions

The unusual phase-change telluride GeTe₂, promising for reconfigurable THz metasurfaces and controlled crystallization, producing functional 2D nanomaterials, was studied as a glassy

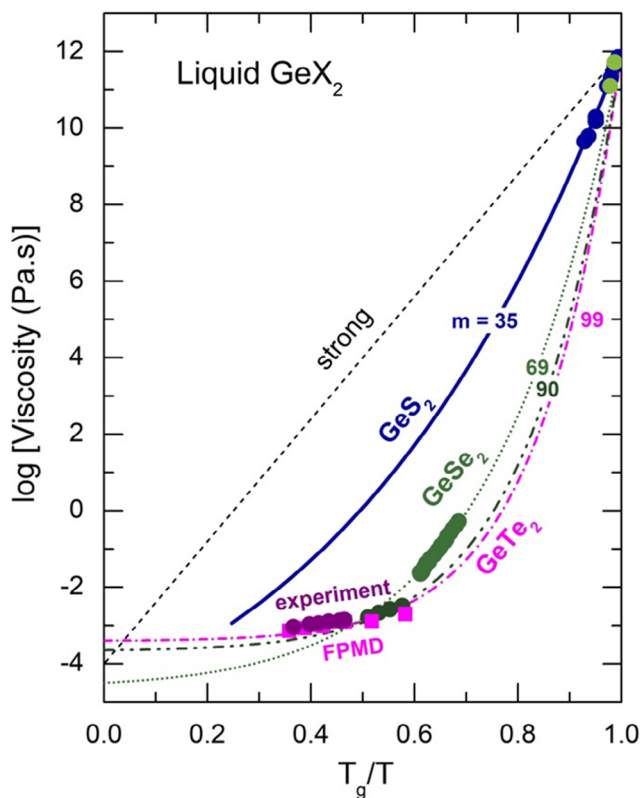


Figure 7. Viscosity of GeS_2 (blue),^[51,66] semiconducting and metallic GeSe_2 (different shades of green),^[49–51] and experimental^[14] and FPMD-derived^[7] GeTe_2 (violet and magenta, respectively). The respective MYEGA^[42] relationships are shown by color-coded solid, dotted, dash-dotted, and dash-dot-dotted lines, together with fragility indices m .

semiconducting PLD film and metallic high-temperature liquids using high-energy X-Ray diffraction and first-principles simulations. The results confirmed the partial disproportionation of glassy GeTe_2 into GeTe and Te , resulting in mixed tetrahedral/trigonal germanium local coordination and Te-Te homopolar bonds. The disproportionation reaction is complete in metallic liquid GeTe_2 , yielding equally populated short Ge-Te(S) and long Ge-Te(L) interatomic distances, along with significant chemical disorder, characterized by Ge-Ge and Te-Te NN contacts. The germanium local structure in metallic liquid resembles that in rhombohedral GeTe but with lower Ge coordination, $5.0 \leq N_{\text{Ge-Te}} N_{\text{Ge-Ge}} \leq +5.3$, and denser packing, as reflected by shorter NN and second-neighbor distances. The high internal pressure in dense metallic liquid, also illustrated by characteristic changes in the FSDP, seems to be the origin of the structural and chemical metastability of the GeTe_2 compound. Similar processes might be operational in archetypical tetrahedral GeS_2 and GeSe_2 under high pressure and temperature.

4. Experimental Section and Computational Details

A crystalline GeTe_2 sample for high-temperature diffraction measurements was synthesized using high-purity elements Ge (99.999%,

Neyco) and Te (99.999%, Cerac) in an evacuated silica tube at ≈ 1220 K in a rocking furnace. Subsequently, a small quantity of the synthesized sample was placed into a silica tube (2 mm ID, 3 mm OD), evacuated, and sealed. The germanium ditelluride target for PLD was prepared in a flat bottom evacuated silica tube of 25 mm ID. Further details of the target preparation can be found elsewhere.^[53] GeTe_2 thin films (≈ 1 μm) were deposited at room temperature by PLD onto glass substrates using a Neocera PLD system equipped with a 248 nm KrF excimer laser (Coherent Compex 102 F).

The removed pieces of the PLD film were placed into a silica capillary for HE-XRD measurements. The room-temperature experiments were conducted at the 6-ID-D beamline of the Advanced Photon Source (Argonne National Laboratory, Chicago), utilizing a photon energy of 99.9593 keV. A 2D setup with a Varex area detector was employed for data collection. The 2D diffraction patterns were processed using the Fit2D software.^[54] The analysis involved subtracting the measured background intensity of the empty silica capillary. Additionally, corrections were applied for the different detector geometries and efficiencies, sample self-attenuation, and Compton scattering using standard procedures.^[55]

A dedicated two-axis diffractometer at the BL04B2 beamline of the SPring-8 facility (Hyogo Prefecture, Japan) was employed for high-temperature HE-XRD measurements. The diffractometer was equipped with four CdTe detectors at low angles and three Ge diodes at high diffraction angles.^[56] The measurements were conducted over the temperature range from 873 to 1223 K in a furnace. An incident X-Ray energy of 112.6386 keV was used, providing a high signal-to-noise ratio and sufficient energy resolution to discriminate both fluorescence from the sample and higher harmonic reflections from the monochromator crystal. The empty silica tube at different temperatures was also measured and used for background intensity subtraction. Further data analysis included absorption, Compton scattering, and polarization corrections following standard procedures.^[57] The resulting total X-Ray structure factor $S_X(Q)$ was then derived.

$$S_X(Q) = w_{\text{GeGe}}(Q)S_{\text{GeGe}}(Q) + w_{\text{GeTe}}(Q)S_{\text{GeTe}}(Q) + w_{\text{TeTe}}(Q)S_{\text{TeTe}}(Q) \quad (2)$$

where $w_{ij}(Q)$ represent the Q -dependent weighing coefficients, and $S_{ij}(Q)$ are the Faber–Ziman partial structure factors. The Fourier transform of $S_X(Q)$ yielded the pair-distribution function $g_X(r)$.

$$g_X(r) = 1 + \frac{1}{2\pi^2 \rho_0 r} \int_0^{Q_{\text{max}}} Q[S_X(Q) - 1] \sin(Qr)M(Q)dQ \quad (3)$$

where ρ_0 is the number density, $M(Q)$ is the Lorch window function, and $Q_{\text{max}} = 25 \text{ \AA}^{-1}$.

Born–Oppenheimer molecular dynamics, implemented within the CP2K package,^[58] was applied to explore the short- and intermediate-range structure as well as atomic dynamics in amorphous and liquid GeTe_2 . The GGA and the PBE0^[23,24] hybrid exchange-correlation functional, augmented by Grimme dispersion corrections D3BJ,^[59] were used. The initial atomic configuration was generated using Reverse Monte Carlo modeling.^[60] The cubic simulation box, containing 450 atoms (150 Ge and 300 Te), was sized to match the experimental density. Subsequent optimization was conducted using density functional theory, employing the molecularly optimized correlation-consistent polarized triple-zeta valence basis set and norm-conserving relativistic Goedecker–Teter–Hutter-type pseudopotentials.^[61] FPMD simulations were carried out using a canonical NVT ensemble with a Nosé–Hoover^[62,63] thermostat. The simulation boxes underwent heating and cooling cycles from 300 to 1300 K using 100 K steps for the duration of 15–50 ps each. The connectivity, ring statistics, and bond angle distributions were analyzed using the R. I. N. G. S. package^[64] and a modified connectivity program.^[65] Further simulation details can be found elsewhere.^[7,31,53]

Supporting Information

Supporting Information is available from the Wiley Online Library or from the author.

Acknowledgements

The work at Littoral was supported by the Région Hauts de France and the Ministère de l'Enseignement Supérieur et de la Recherche (CPER ECRIN), as well as by the European Fund for Regional Economic Development. The experiments at SPring-8 were approved by the Japan Synchrotron Radiation Research Institute (proposal nos. 2021A1432 and 2022A1418) and supported by the Centre for Advanced Science and Technology (Japan). Work at the Advanced Photon Source, Argonne National Laboratory, was supported in part by the Office of Basic Energy Sciences, US Department of Energy, under contract no. DEAC02-06CH11357. S.B.'s work was supported by the project TK210, Center of Excellence in Sustainable Green Hydrogen and Energy Technologies", and by Education and Youth Board of Estonia in frames of ÖÜF5 project. M.K.'s work was supported by the Ministry of Science and Higher Education within the State assignment of the NRC "Kurchatov Institute". The FPMD simulations were carried out using the HPC computing resources at Lomonosov Moscow State University. This work was also granted access to the HPC resources of IDRIS (France) under the allocation 2023-A0150910639 made by Grand Equipement National de Calcul Intensif (GENCI) and to use the CALCULCO computing platform, supported by Service Commun du Système d'Information de l'Université du Littoral Côte d'Opale (SCoSI/ULCO).

Conflict of Interest

The authors declare no conflict of interest.

Data Availability Statement

The data that support the findings of this study are available from the corresponding author upon reasonable request.

Keywords

atomic structures, phase-change materials, semiconductor–metal transition | viscosities

Received: December 22, 2023

Revised: January 13, 2024

Published online:

- [1] M. Wuttig, N. Yamada, *Nat. Mater.* **2007**, *6*, 824.
 [2] S. Raoux, W. Welnic, D. Ielmini, *Chem. Rev.* **2010**, *110*, 240.
 [3] W. Zhang, R. Mazzarello, M. Wuttig, E. Ma, *Nat. Rev. Mater.* **2019**, *4*, 150.
 [4] C. Rios, N. Youngblood, Z. Cheng, M. Le Gallo, W. H. P. Pernice, C. D. Wright, A. Sebastian, H. Bhaskaran, *Sci. Adv.* **2019**, *5*, eaau5759.
 [5] J. Feldmann, N. Youngblood, M. Karpov, H. Gehring, X. Li, M. Stappers, M. Le Gallo, X. Fu, A. Lukashchuk, A. S. Raja, J. Liu, C. D. Wright, A. Sebastian, T. J. Kippenberg, W. H. P. Pernice, H. Bhaskaran, *Nature* **2021**, *589*, 52.
 [6] M. Y. Shalaginov, S. An, Y. Zhang, F. Yang, P. Su, V. Liberman, J. B. Chou, C. M. Roberts, M. Kang, C. Rios, et al., *Nat. Commun.* **2021**, *12*, 1225.

- [7] A. Tverjanovich, M. Khomenko, C. J. Benmore, M. Bokova, A. Sokolov, D. Fontanari, M. Kassem, T. Usuki, E. Bychkov, *Chem. Mater.* **2021**, *33*, 1031.
 [8] M. R. Konnikova, M. D. Khomenko, A. S. Tverjanovich, S. Bereznev, A. A. Mankova, O. D. Parashchuk, I. S. Vasilevsky, I. A. Ozheredov, A. P. Shkurinov, E. A. Bychkov, *ACS Appl. Mater. Interfaces* **2023**, *15*, 9638.
 [9] Y. Saito, S. Hatayama, W. H. Chang, N. Okada, T. Irisawa, F. Uesugi, M. Takeguchi, Y. Sutou, P. Fons, *Mater. Horiz.* **2023**, *10*, 2254.
 [10] E. Bychkov, M. Miloshova, D. L. Price, C. J. Benmore, A. Lorriaux, *J. Non-Cryst. Solids* **2006**, *352*, 63.
 [11] J. A. Kalb, M. Wuttig, F. Spaepen, *J. Mater. Res.* **2007**, *22*, 748.
 [12] P. Lucas, W. Takeda, J. Pries, J. Benke-Jacob, M. Wuttig, *J. Chem. Phys.* **2023**, *158*, 054502.
 [13] Y. Tsuchiya, *J. Phys. Soc. Jpn.* **1991**, *60*, 227.
 [14] V. M. Glazov, S. N. Chizhevskaya, N. N. Glagoleva, *Liquid Semiconductors (Zhidkie Poluprovodniki)*, Nauka, Moscow **1967**, p. 198.
 [15] J. Ruska, H. Thurn, *J. Non-Cryst. Solids* **1976**, *22*, 277.
 [16] T. Okada, T. Satoh, M. Matsumura, S. Ohno, *J. Phys. Soc. Jpn.* **1996**, *65*, 230.
 [17] Y. Kameda, O. Uemura, T. Usuki, *Mater. Trans. JIM* **1996**, *37*, 1655.
 [18] K. Maruyama, H. Ebata, S. Suzuki, M. Misawa, S. Takeda, Y. Kawakita, *J. Non-Cryst. Solids* **1999**, *250–252*, 483.
 [19] I. Kaban, P. Jónvári, W. Hoyer, R. G. Delaplane, A. Wannberg, *J. Phys.: Condens. Matter* **2006**, *18*, 2749.
 [20] M. H. Bhat, V. Molinero, E. Soignard, V. C. Solomon, S. Sastry, J. L. Yarger, C. A. Angell, *Nature* **2007**, *448*, 787.
 [21] J. Akola, R. O. Jones, S. Kohara, T. Usuki, E. Bychkov, *Phys. Rev. B* **2010**, *81*, 094202.
 [22] L. Zhong, J. Wang, H. Sheng, Z. Zhang, S. X. Mao, *Nature* **2014**, *512*, 177.
 [23] J. P. Perdew, M. Ernzerhof, K. Burke, *J. Chem. Phys.* **1996**, *105*, 9982.
 [24] C. Adamo, V. Barone, *J. Chem. Phys.* **1999**, *110*, 6158.
 [25] W. A. Crichton, M. Mezouar, T. Grande, S. Stølen, A. Grzechnik, *Nature* **2001**, *414*, 622.
 [26] V. V. Brazhkin, Y. Katayama, M. V. Kondrin, A. G. Lyapin, H. Saitoh, *Phys. Rev. B* **2010**, *82*, 140202.
 [27] E. Soignard, O. B. Tsiok, A. S. Tverjanovich, A. Bychkov, A. Sokolov, V. V. Brazhkin, C. J. Benmore, E. Bychkov, *J. Phys. Chem. B* **2020**, *124*, 430.
 [28] C. Otjacques, J.-Y. Raty, F. Hippert, H. Schober, M. Johnson, R. Céolin, J.-P. Gaspard, *Phys. Rev. B* **2010**, *82*, 054202.
 [29] S. Wei, M. Stolpe, O. Gross, W. Hembree, S. Hechler, J. Bednarcik, R. Busch, P. Lucas, *Acta Mater.* **2017**, *129*, 259.
 [30] M. Kassem, C. J. Benmore, T. Usuki, K. Ohara, A. Tverjanovich, M. Bokova, V. V. Brazhkin, E. Bychkov, *J. Phys. Chem. Lett.* **2022**, *13*, 10843.
 [31] M. Bokova, A. Tverjanovich, C. J. Benmore, D. Fontanari, A. Sokolov, M. Khomenko, M. Kassem, I. Ozheredov, E. Bychkov, *ACS Appl. Mater. Interfaces* **2021**, *13*, 37363.
 [32] I. Petri, P. S. Salmon, W. S. Howells, *J. Phys.: Condens. Matter* **1999**, *11*, 10219.
 [33] G. Dittmar, H. Schäfer, *Acta Crystallogr. B* **1975**, *31*, 2060.
 [34] G. Dittmar, H. Schäfer, *Acta Crystallogr. B* **1976**, *32*, 2726.
 [35] H. Wiedemeier, H. G. von Schnering, *Z. Kristallg.* **1978**, *148*, 295.
 [36] F. Serrano-Sánchez, M. Funes, N. M. Nemes, O. J. Dura, J. L. Martínez, J. Prado-Gonjal, M. T. Fernández-Díaz, J. A. Alonso, *Appl. Phys. Lett.* **2018**, *113*, 083902.
 [37] A. Schlieper, Y. Feutelais, S. G. Fries, B. Legendre, R. Blachnik, *CALPHAD* **1999**, *23*, 1.
 [38] S. Susman, K. J. Volin, D. G. Montague, D. L. Price, *J. Non-Cryst. Solids* **1990**, *125*, 168.

- [39] I. Petri, P. S. Salmon, H. E. Fisher, *Phys. Rev. Lett.* **2000**, *84*, 2413.
- [40] M. Micoulaut, R. Vuilleumier, C. Massobrio, *Phys. Rev. B* **2009**, *79*, 214205.
- [41] G. W. Scherer, *J. Am. Ceram. Soc.* **1992**, *75*, 1060.
- [42] J. C. Mauro, Y. Yue, A. J. Ellison, P. K. Gupta, D. C. Allan, *Proc. Natl. Acad. Sci. USA* **2009**, *106*, 19780.
- [43] C. A. Angell, *Science* **1995**, *267*, 1924.
- [44] C. A. Angell, *Chem. Rev.* **2002**, *102*, 2627.
- [45] J. Orava, D. W. Hewak, A. L. Greer, *Adv. Funct. Mater.* **2015**, *25*, 4851.
- [46] S. Wei, P. Lucas, C. A. Angell, *J. Appl. Phys.* **2015**, *118*, 034903.
- [47] W. Zhu, O. Gulbitten, B. Aitken, S. Sen, *J. Non-Cryst. Solids* **2021**, *554*, 120601.
- [48] J. Pries, H. Weber, J. Benke-Jacob, I. Kaban, S. Wei, M. Wuttig, P. Lucas, *Adv. Funct. Mater.* **2022**, 2202714.
- [49] V. M. Glazov, O. V. Situlina, *Dokl. Akad. Nauk SSSR* **1969**, *187*, 799.
- [50] A. Laugier, G. Chaussemy, J. Fornazero, *J. Non-Cryst. Solids* **1977**, *23*, 419.
- [51] A. S. Tverjanovich, *Glass Phys. Chem.* **2003**, *29*, 532.
- [52] V. A. Ananichev, *Bulk Dilatometry of Chalcogenide Glassy Materials*, St. Petersburg Polytechnical University, St Petersburg **2007**, pp. 151–152.
- [53] A. Tverjanovich, M. Khomenko, C. J. Benmore, S. Bereznev, A. Sokolov, D. Fontanari, A. Kiselev, A. Lotin, E. Bychkov, *J. Mater. Chem. C* **2021**, *9*, 17019.
- [54] A. P. Hammersley, S. O. Svensson, M. Hanfland, A. N. Fitch, D. Häusermann, *High Pressure Res.* **1996**, *14*, 235.
- [55] L. B. Skinner, C. J. Benmore, J. B. Parise, *Nucl. Instrum. Methods Phys. Res.* **2012**, *662*, 61.
- [56] K. Ohara, Y. Onodera, S. Kohara, C. Koyama, A. Masuno, A. Mizuno, J. T. Okada, S. Tahara, Y. Watanabe, H. Oda, Y. Nakata, H. Tamaru, T. Ishikawa, O. Sakata, *Intern. J. Microgravity Sci. Appl.* **2020**, *37*, 370202.
- [57] S. Kohara, M. Itou, K. Suzuya, Y. Inamura, Y. Sakurai, Y. Ohishi, M. Takata, *J. Phys.: Condens. Matter* **2007**, *19*, 506101.
- [58] T. D. Kühne, M. Iannuzzi, M. Del Ben, V. V. Rybkin, P. Seewald, F. Stein, T. Laino, R. Z. Khaliullin, O. Schütt, F. Schiffmann, D. Golze, J. Wilhelm, S. Chulkov, M. H. Bani-Hashemian, V. Weber, U. Borštnik, M. Taillefumier, A. S. Jakobovits, A. Lazzaro, H. Pabst, T. Müller, R. Schade, M. Guidon, S. Andermatt, N. Holmberg, G. K. Schenter, A. Hehn, A. Bussy, F. Belleflamme, et al., *J. Chem. Phys.* **2020**, *152*, 194103.
- [59] S. Grimme, S. Ehrlich, L. Goerigk, *J. Comput. Chem.* **2011**, *32*, 1456.
- [60] O. Gereben, L. Pusztai, *J. Comput. Chem.* **2012**, *33*, 2285.
- [61] C. Hartwigsen, S. Goedecker, J. Hutter, *Phys. Rev. B* **1998**, *58*, 3641.
- [62] S. Nosé, *Mol. Phys.* **1984**, *52*, 255.
- [63] W. G. Hoover, *Phys. Rev. A* **1985**, *31*, 1695.
- [64] S. Le Roux, P. Jund, *Comput. Mater. Sci.* **2010**, *49*, 70.
- [65] S. Kohara, H. Ohno, M. Tabaka, T. Usuki, H. Morita, K. Suzuya, J. Akola, L. Pusztai, *Phys. Rev. B* **2010**, *82*, 134209.
- [66] J. Málek, J. Shanelova, *J. Non-Cryst. Solids* **1999**, *243*, 116.